THE JOURNAL OF PHYSICAL CHEMISTRY B

ARTICLE

pubs.acs.org/JPCB

Analysis of Infrared Spectra of β-Hairpin Peptides As Derived from Molecular Dynamics Simulations

Laura Zanetti Polzi,[†] Isabella Daidone,[‡] Massimiliano Anselmi,[†] Giuliano Carchini,[†] Alfredo Di Nola,[†] and Andrea Amadei*[,§]

[†]Dipartimento di Chimica, University of Rome "La Sapienza", Rome, Italy

[‡]Dipartimento di Chimica Ingegneria Chimica e Materiali, University of L'Aquila, Coppito (AQ), Italy

[§]Dipartimento di Scienze e Tecnologie Chimiche, University of Rome "Tor Vergata", Rome, Italy

ABSTRACT: Infrared temperature-dependent spectroscopy is a well-known tool to characterize folding/unfolding transitions in peptides and proteins, assuming that the higher the temperature, the higher the unfolded population. The infrared spectra at different temperatures of two β-hairpin peptides (gramicidin S analogues GS6 and GS10) are here reconstructed by means of molecular dynamics (MD) simulations and a theoretical−computational method based on the perturbed matrix method. The calculated temperature-dependent spectra result in good agreement with the experimental available spectra. The same methodology has been then used to reconstruct the spectra corresponding to the pure unfolded and folded states, as defined from the MD simulations, in order to better understand the temperature-dependent spectra and to help the interpretation of the experimental spectra. For example, our results show that in the case of the GS6 peptide the analysis of the temperature-dependent spectra cannot be used to investigate the folding/unfolding kinetics within the usual assumption that the higher the temperature, the higher the probability of the unfolded state.

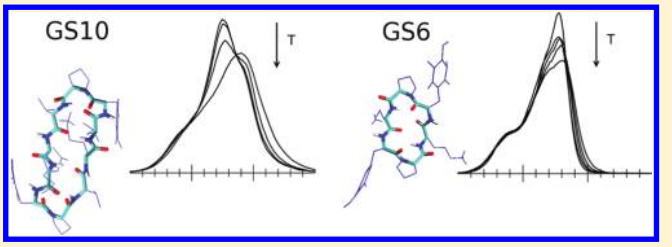

INTRODUCTION

One of the most interesting problems of protein biophysics concerns the pathways of conformational transitions in protein folding. Small size and structural simplicity make short peptides that fold into well-defined structures ideal model systems for examining the factors that govern protein folding.[1] Of particular interest are β-hairpins because, despite their small size (typically less than 20 residues), they exhibit various properties that are typical in globular proteins, e.g., they may contain a hydrophobic core and/or exhibit a cooperative thermal folding/unfolding transition.[2,3]

Although experimental measurements of the folding kinetics of β-hairpins are scarce,[2,4−8] in the past decade a remarkable number of theoretical and computational studies have been conducted to investigate hairpin structure, stability, and folding transitions.[3,9−17] Molecular dynamics (MD) simulations have proven to be a powerful tool for the investigation of the atomistic behavior of solvated β-hairpin peptides, including structural/conformational transitions[18−20] and, more recently, even folding/unfolding kinetics and thermodynamics.[21−23]

Various experimental techniques have been used to characterize the folding/unfolding process, for example, fluorescence resonance energy transfer (FRET), small-angle X-ray scattering (SAXS), circular dichroism, and real-time NMR.[24,25] Among the others, Fourier transform infrared (FTIR) spectroscopy has been widely used to study peptides and proteins secondary structures under equilibrium conditions.[26,27] This spectroscopic technique has been further developed to study unfolding or refolding transitions in peptides initiated by temperature jump (T-jump) using time-resolved infrared (TRIR) spectroscopy.[27,28] Amide group vibrational modes of the backbone are typically used in peptide infrared spectroscopy because of their sensitivity to secondary structure and solvation changes. In particular the amide I mode, essentially corresponding to the C═O stretch (1600−1700 cm^{-1}), is by far the most studied. Despite the fact that IR spectroscopy has been used extensively to obtain structural information of numerous peptides and proteins in solution, this method has the limitation that the band shapes for different secondary structures may be similar to one another and highly congested,[29] thus leading to spectra which are difficult to understand in terms of structures and conformational changes.

In the last years many different theoretical−computational methods have been proposed to model protein and peptide IR spectroscopic behavior, the development and parametrization of which is at present an active area of research.[29−40] These methods provided a proper reproduction of some spectroscopic features of the folded state, taking into account the symmetry of the folded structure, e.g., β-sheet. On the contrary, much less information about the spectroscopic features of the unfolded state are available, although unfolded state spectroscopy is experimentally widely used to monitor folding/unfolding transitions.

Received: March 11, 2011
Revised: September 1, 2011
Published: September 06, 2011

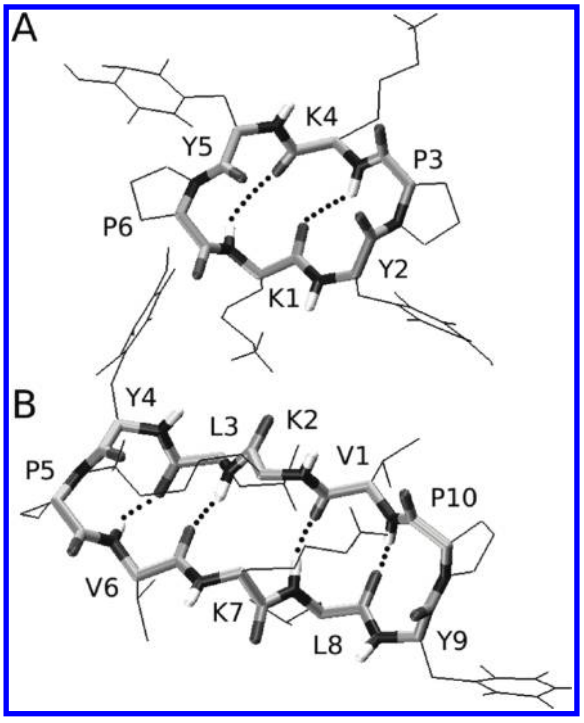

Figure 1. Snapshots of the β-hairpin structure of GS6 (panel A) and GS10 (panel B) extracted from MD runs. Hydrogen bonds are represented with dotted lines.

In this paper the IR spectra of two β-hairpin peptides, for which experimental spectra are available, are computationally reconstructed by means of a theoretical−computational approach based on the perturbed matrix method (PMM),[41−44] in order to clarify the relationship between conformational and spectroscopic features and to shed light on folding/unfolding transitions.

The PMM method is a mixed quantum mechanics/molecular dynamics (QM/MD) method that keeps the configurational complexity of the system with a proper treatment of the quantum degrees of freedom of its portion to be explicitly described at the electronic level (the quantum center). The main aim of the application of the PMM method to the calculation of infrared spectra is the reproduction of the essential physics underlying IR excitations without involving any phenomenological parameter. One of the advantages of this methodology is that, as the method relies on classical MD for the phase space sampling, a statistically relevant sampling of the quantum-center/environment configurations can be achieved, which is necessary for the calculation of the spectra of complex systems, such as amyloids and peptides or proteins unfolded states.[45−47] Moreover, the amide I signal arising from any peptide residue may be isolated and the effect of the excitonic coupling on the spectrum features quantified. However, as the methodology does not make use of empirical/adjustable parameters, it might be less accurate in reproducing some of the details of the spectroscopic signals compared to other methodologies.[48−50] The main differences between the PMM approach and other methodologies available for the calculation of IR spectra have been previously discussed more in detail.[46,51]

Starting from all-atoms MD simulations, PMM calculations provide here the IR temperature-dependent spectrum of two cyclic β-hairpin peptides belonging to the same family: a 6-meric (GS6) and a 10-meric (GS10) analogue of gramicidin S, with structures presented in Figure 1. The results obtained are finally compared to the available experimental data obtained by means of temperature-dependent FTIR spectroscopy.[4]

THEORY

The methodology used here to reconstruct the amide I′ (amide I in D_2O) infrared spectra of the two β-hairpin peptides has been explained in detail in previous articles.[45,46] Hereafter, the theoretical basis of PMM calculations and the computational procedure used to obtain vibrational spectra of solvated peptides are briefly outlined.

In PMM calculations,[41−44,52] similarly to other mixed quantum-classical procedures,[53−55] it is essential to predefine a portion of the system to be treated at the electronic level, hereafter termed as the quantum center (QC), with the rest of the system described at a classical atomistic level exerting the perturbation on the QC electronic states.

The QC used here to model each peptide group along the peptide backbone is *trans*-*N*-methylamide (NMA). An orthonormal set of unperturbed electronic Hamiltonian ($\tilde{H}^0$) eigenfunctions (ϕ_j^0) are initially evaluated on the QC structure of interest (see Methods). Then, after *trans*-NMA has been fitted on the given peptide group, the perturbed electronic ground state energy is calculated for each peptide group with the following procedure. Indicating with $\mathcal{V}$ and $\mathcal{E}$ the perturbing electric potential and field, respectively, exerted by the environment on the QC (typically obtained by the environment atomic charge distribution and evaluated in the QC center of mass) the perturbed electronic Hamiltonian ($\tilde{H}$) for each QC-environment configuration (as generated by the MD simulation) can be constructed

$$\tilde{H} \simeq \tilde{H}^0 + \tilde{I} q_T \mathcal{V} + \tilde{Z}_1 + \Delta V \tilde{I}$$

$$[\tilde{Z}_1]_{j,j'} = -\mathbf{E}\cdot\langle\phi_j^0|\hat{\boldsymbol{\mu}}|\phi_{j'}^0\rangle$$

where q_T, $\hat{\boldsymbol{\mu}}$, and ϕ_j^0 are the QC total charge, dipole operator, and unperturbed electronic eigenfunctions, respectively, ΔV approximates all the higher order terms as a simple short-range potential, $\tilde{I}$ is the identity matrix, and the angled brackets indicate integration over the electronic coordinates. The diagonalization of $\tilde{H}$ provides a set of eigenvectors and eigenvalues representing the QC perturbed electronic eigenstates and energies. Note that the side chain of the considered peptide group, the $N - 1$ residues, and the solvent define the perturbing environment at each configuration generated by the MD simulation; every structural change (i.e., hydrogen bonding) will thus be taken into account by means of the perturbing local electric field acting on the QC. Then, via a polynomial fit of the perturbed electronic ground state energy along the mode coordinate, the perturbed frequencies for each oscillator along the peptide at each MD frame can be obtained.

The basic approximation of the methodology presented so far is that, for typical quantum vibrational degrees of freedom, the environment perturbation does not significantly alter the vibrational modes (i.e., the mass-weighted QC Hessian eigenvectors) but only the related eigenvalues. Such an assumption provides a good approximation when, under the perturbation, a vibrational mode remains largely uncoupled from the other QC modes as well as from the vibrational modes of the solvent molecules.

When modes coupling effects due to interacting vibrational centers cannot be neglected, excitonic effects must be included in the calculations. The perturbed frequencies for each oscillator are thus used to include the excitonic effect by the construction and diagonalization of the excitonic Hamiltonian matrix (i.e., the Hamiltonian matrix for the interacting chromophores) given by[44]

$$\tilde{H} = \tilde{I}U_{\mathrm{vb},0} + \Delta\tilde{H}$$

with $U_{\mathrm{vb},0}$ the (vibronic) ground state energy of the interacting chromophores and $\Delta\tilde{H}$ the excitation matrix[46] whose diagonal elements are

$$[\Delta\tilde{H}]_{kl,kl} = h\nu_{kl}$$

and whose nonzero off-diagonal elements are given by the chromophores interaction operator (within the dipolar approximation)

$$\hat{V}_{k,k'(k\neq k')} = \frac{\hat{\boldsymbol{\mu}}_k \cdot \hat{\boldsymbol{\mu}}_{k'}}{R^3_{k,k'}} - 3\frac{(\hat{\boldsymbol{\mu}}_k \cdot \mathbf{R}_{k,k'})(\hat{\boldsymbol{\mu}}_{k'} \cdot \mathbf{R}_{k,k'})}{R^5_{k,k'}}$$

with ν_{kl} the kth chromophore lth excitation frequency, $\hat{\mu}_k$ the kth chromophore dipole operator, and $\mathbf{R}_{k,k'}$ the k' to k chromophore displacement vector defined by the corresponding chromophores origins. In the previous equation for each chromophore only the first vibrational excitation of the electronic ground state must be involved, as higher vibrational excitations are forbidden and the coupling with excited electronic states may be neglected. By diagonalizing the excitation matrix and using the transition dipole for the $0 \rightarrow i$ excitonic transition ($\mu_{0,i}$) as obtained via the excitonic eigenvectors, we may reconstruct the spectral signal of the excitonic system by summing the absorbance due to each $0 \rightarrow i$ transition, providing

$$\varepsilon(\nu) = \sum_i \frac{|\boldsymbol{\mu}_{0,i}|^2 \rho_i(\nu) h\nu}{6\varepsilon_0 c\hbar^2}$$

with ρ_i the probability density in ν frequency space for the ith excitation and ε_0 the vacuum dielectric constant.

METHODS

Unperturbed Quantum Chemical Calculations. As a model of the peptide group, i.e., the quantum center to be explicitly treated at the electronic level, *trans*-NMA is chosen. Quantum chemical calculations are carried out on the isolated *trans*-NMA molecule with time-dependent density functional theory (TDDFT) with the 6-31+G(d) basis set. This level of theory is selected because it represents a good compromise between computational costs and accuracy. The mass-weighted Hessian matrix is calculated on the optimized geometry at the B3LYP/6-31+G(d) level of theory and subsequently diagonalized for obtaining the unperturbed eigenvectors and related eigenvalues. The eigenvector corresponding in vacuo to the amide I′ mode is, then, used to generate a grid of points (i.e., configurations) as follows: a step of 0.05 au is adopted and the number of points is set to span an energy range of 20 KJ/mol (in the present case 31 points). For each point, six unperturbed electronic states are then evaluated at the same level of theory providing the basis set for the PMM calculations.

Molecular Dynamics Simulations. The initial structure of *cyclo*-[(Lys-dTyr-Pro)$_2$] and *cyclo*-[(Val-Lys-Leu-dTyr-Pro)$_2$] are created using Pymol version 0.99 (DeLano Scientific) on the basis of the experimental chemical structure.[56,57] Geometry optimization of that structure is done by using the empirical potential energy function of the GROMOS96 43a1 force field.[58] The peptide, in its starting conformation, is solvated with water and placed in a periodic cubic box large enough to contain the peptide and 0.5 nm of solvent on all sides. The two lysine side chains are protonated as to reproduce a pH of about 7: two negative counterions (Cl^-) are then added by replacing two water molecules to achieve a neutral condition. MD simulations, in the NVT ensemble, with fixed bond lengths[59] are performed with the GROMACS software package[60] and with the GROMOS96 43a1 force field. Water is modeled using the deuterated simple point charge (SPC) water model.[61] A nonbonded pair-list cutoff of 9.0 Å is used, and the long-range electrostatic interactions are treated with the particle mesh Ewald method.[62] Isokinetic temperature coupling[63] is used to keep the temperature constant at the desired value.

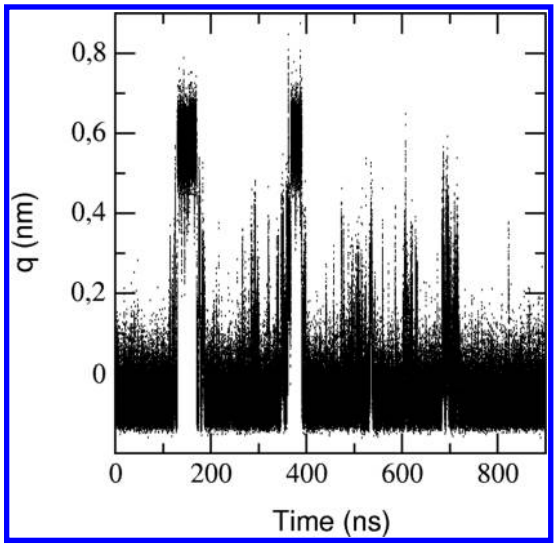

Figure 2. Time evolution of the projection of the MD trajectory at 330 K on the first eigenvector of the covariance matrix of the distances between the oxygen and nitrogen atoms involved in the four H-bonds of GS10.

After various equilibration MD runs, all-atoms (with the exception of nonpolar hydrogens) simulations in explicit water at different temperatures and with different time lengths are carried out for the two peptides as follows.

GS6 : 400 ns at 280 K, 300 ns at 310 K,
300 ns at 360 K, 180 ns at 400 K, 60 ns at 500 K

GS10 : 200 ns at 280 K, 300 ns at 310 K,
900 ns at 330 K, 490 ns at 400 K

For the simulation at 500 K, a time step of 1 fs is used, while for the others the time step is 2 fs.

The folded and unfolded conformations for the two peptides are defined via the hydrogen bonds (H-bonds) that characterize the hairpin. In the case of GS6, there are two H-bonds and, as previously described in detail,[23] the secondary structure states are defined by projecting the MD trajectories onto the plane defined by the two distances between the oxygen and nitrogen atoms involved in the two H-bonds. The folded and unfolded conformational states are identified: in the folded state both H-bonds

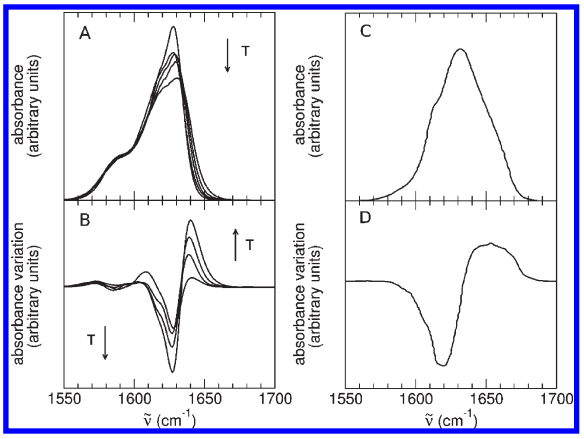

Figure 3. Panel A: Computed IR spectra in the amide I′ region of GS6 in D_2O solution at 280, 310, 360, 400, and 500 K. Panel B: Difference spectra obtained by subtracting the spectrum calculated at 280 K from the spectra calculated at higher temperatures. Panel C: Reproduction of the experimental absorbance spectrum obtained by Maness et al.[4] at an intermediate temperature in the range experimentally examined. Panel D: Reproduction of the experimental absorbance variation spectrum obtained by Maness et al.[4] at an intermediate temperature in the range experimentally examined.

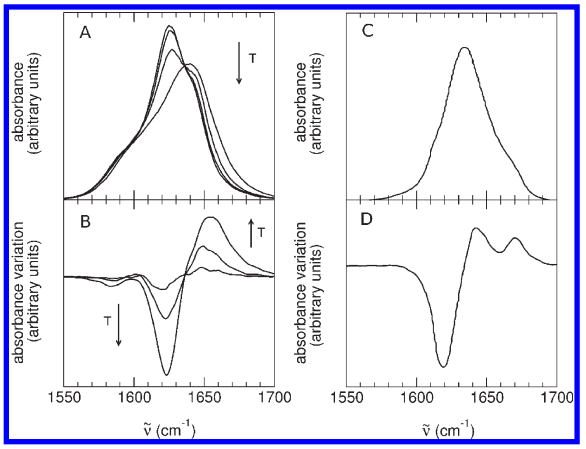

Figure 4. Panel A: Computed IR spectra in the amide I′ region of GS10 in D_2O solution at 280, 310, 330, and 400 K. Panel B: Difference spectra obtained by subtracting the spectrum calculated at 280 K from the spectra calculated at higher temperatures. Panel C: Reproduction of the experimental absorbance spectrum obtained by Maness et al.[4] at an intermediate temperature in the range experimentally examined. Panel D: Reproduction of the experimental absorbance variation spectrum obtained by Maness et al.[4] at an intermediate temperature in the range experimentally examined.

are formed, and in the unfolded state none of the two H-bonds is formed.

In the case of GS10, there are four hydrogen bonds. Coherently with the definition used for the smaller peptide, the folded and unfolded conformations are defined using the H-bond distances. The MD trajectories have been projected along the eigenvector corresponding to the largest eigenvalue obtained by diagonalizing the covariance matrix of the distances between the oxygen and nitrogen atoms involved in the four H-bonds. Such an eigenvector defines a conformational coordinate (q) providing the largest concerted H-bonds fluctuations and hence well describing the peptide folding/unfolding transitions.

Figure 2 shows the time course of the q conformational coordinate obtained from the MD trajectory at 330 K, clearly indicating the folding/unfolding transitions. From the observation of the figure two evident transitions from the folded (q values centered at ≈0 nm) to the unfolded (q values centered at ≈0.6 nm) state can be observed. It is also worth to note that in the central part of the trajectory q assumes values in the range between 0.1 and 0.5 nm. These values correspond to an intermediate state in which the four hydrogen bonds are not all stable at the same time. It can be then defined as a mixed state, which we will refer hereafter as to the nonfolded state, in which both the unfolded and the intermediate state are present. The presence of a number of transitions between the previously defined states, together with the small dimensions and cyclicity of the peptides that let us presume that no relevant conformational changes are possible, ensure us that molecular dynamics trajectories of hundreds of nanoseconds (see above) provide a sufficient sampling of the conformational states considered.

RESULTS AND DISCUSSION

The amide I′ temperature-dependent spectra of GS6 and GS10 are here reconstructed starting from the simulation trajectories and compared with the experimental ones obtained by Maness et al.[4]

The experimental IR spectra of GS6 and GS10 show a peak centered at ≈1630 cm^{-1} (1628 cm^{-1} in the case of GS6 and 1634 cm^{-1} in the case of GS10), corresponding to the amide I′ band (see Figure 1 and 2 of ref 4). This peak is experimentally studied at different temperatures (from 2 to 85 °C) by means of equilibrium FTIR spectroscopy in order to characterize the folding and unfolding kinetics, within the usual assumption that at the extreme temperatures the population is either fully folded (2 °C) or fully unfolded (85 °C). As the temperature increases, the peak shifts to higher frequencies and its intensity decreases: consequently, the difference spectra obtained by subtracting the spectrum at the lowest temperature from the ones at higher temperatures exhibit a negative−positive trend along the frequency axis.

The corresponding computed spectra for GS6 obtained at five different temperatures (280, 310, 360, 400, and 500 K) are presented in Figure 3 (panel A). In the same figure (panel B), the temperature difference spectra obtained by subtracting the spectrum at 280 K from the spectra at higher temperatures are also shown. In panels C and D an example of the spectra obtained by Maness et al. is reported by showing the experimental absorbance spectrum and absorbance variation spectrum at an intermediate temperature in the range experimentally examined. Comparison of panel A of this figure with the corresponding experimental data (Figure 1 of ref 4) clearly indicates that the PMM/MD procedure well reproduces the experimental results, properly providing the spectrum shape (including the shoulder on the left of the main peak), the full width at half-maximum (≈30 cm^{-1} in the computed spectrum vs ≈40 cm^{-1} in the experimental one), and the temperature trend. Note that the last two spectra correspond to temperatures beyond the range experimentally analyzed. Also the temperature difference spectra presented in panel B show the same trend of the experimental ones, although the positive component of the absorbance variation is broader in the experimental spectra than in the calculated ones. This discrepancy depends on a slight difference in the high-frequency zone of the absorbance spectra: given that difference spectra are extremely sensitive to the shape details of the spectral high-frequency tails, such slight difference is amplified in the absorbance variation spectra. These kinds of minor variations

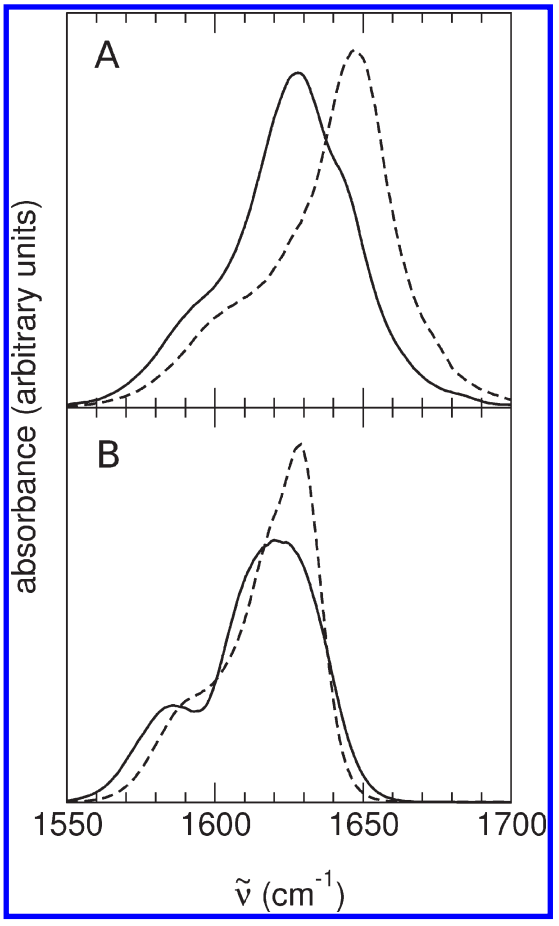

Figure 5. Panel A: Computed IR spectra in the amide I′ region of GS10 in D_2O solution at 330 K in the folded state (solid line) and in the nonfolded state (dashed line). The nonfolded state is a mixed state in which both the unfolded and the intermediate state are present (see Methods). Panel B: Computed IR spectra in the amide I′ region of GS6 in D_2O solution at 310 K in the folded state (solid line) and in the unfolded state (dashed line).

between the calculated and experimental spectra are indicative of the limits of the theoretical model utilized.

The spectra in Figure 3, panels A and B, have been uniformly shifted to lower frequencies by ≈94 cm^{-1} in order to align the computed amide I′ band with the experimental maximum. Such a shift, largely due to the inaccuracies of the ab initio calculations, has been applied to all the computed GS6 IR signals reported in this paper.

The temperature-dependent spectra of GS10 are also reconstructed: in Figure 4 (panel A) the spectra obtained at 280, 310, 330, and 400 K are reported (to be compared with Figure 2 of ref 4). In this case too, the last temperature is beyond the experimental range, and there is a good agreement between the experimental and the calculated spectra, both in the temperature trend (see panel A and the corresponding experimental data[4]) and in the full width at half-maximum (≈40 cm^{-1} in the experimental spectrum and ≈38 cm^{-1} in the calculated one). Similarly to GS6, all the computed GS10 spectra have been shifted to lower frequencies by ≈84 cm^{-1} in order to align the obtained amide I′ band with the experimental maximum. In panels C and D of Figure 4 an example of the spectra obtained by Maness et al. is reported by showing the experimental absorbance spectrum and absorbance variation spectrum at an intermediate temperature in the range experimentally examined.

It is worth to note that in both the GS10 experimental and calculated spectra, the shoulder on the left of the main peak is less evident than in the case of GS6. Moreover, the positive peaks of the temperature-dependent difference spectra result aligned in frequency in the case of GS6 (in the experimental as well as in the calculated spectra, Figure 3, panel B) while they shift to higher frequencies with the raising of the temperature in the case of GS10 (Figure 4, panel B).

In the experimental temperature difference spectra of GS10, a second small positive peak can be observed, which is not present in our calculated spectra. This secondary peak arises from a shoulder in the high-frequency region of the absorbance spectra of GS10 we do not reproduce by means of our calculations, possibly due to inaccuracies in the classical force field and/or in the ab initio calculations. However, as many details of the spectral signal of these peptides have been very well reproduced by the PMM calculations, it is possible that the missing secondary peak arises from different solution conditions between the calculations and the experiments. For example, this peak could also be due to amide dipole coupling arising from peptide−peptide intermolecular interactions we disregarded in our calculations as in this paper we consider peptides at infinite dilution conditions.

In panel A of Figure 5 the spectra corresponding to the folded and the nonfolded state (i.e., a mixture of the unfolded and the intermediate state, see Methods) are reported for GS10 at 330 K. A ≈15−20 cm^{-1} upshift of the peak maximum of the nonfolded state with respect to the peak of the folded state can be observed.

Comparing the spectra of Figure 5, panel A, with the temperature-dependent spectra of GS10 (Figure 4, panel A), the transition from the folded to the nonfolded state can be observed with the raising of the temperature. In fact, the low-temperature spectra (280 and 310 K) correspond to the folded state spectrum, and the highest temperature spectrum (400 K) mainly corresponds to the nonfolded one (the frequency of the main peak shifts toward higher frequencies by ≈15−20 cm^{-1}). Note that in the spectrum at 330 K a shoulder appears on the right of the main peak corresponding to a mixture of the folded and nonfolded state. In fact, this temperature has been experimentally identified as the melting one. The fact that the higher the temperature, the higher the population of the nonfolded state is further confirmed by the analysis of the hydrogen bonds pattern at every temperature (data not shown).

In Figure 5, panel B, the computed spectra of the unfolded and folded state of GS6 at 310 K are reported. The spectrum of the folded state of GS6 is characterized by a pronounced shoulder on the left of the main peak. This shoulder has been shown to depend on the excitonic coupling between the vibrational centers,[46] and its intensity in the case of GS6 is likely to depend on the cyclicity and small dimensions of the peptide: the vibrational centers are very close one to each other and their relative positions are forced to be almost fixed. This leads to a very strong excitonic effect. Moreover, a less evident shoulder can be observed in the unfolded state spectrum showing that, this peptide being so small and cyclic, also the unfolded state is structurally rather rigid indicating a significant excitonic coupling. This is also confirmed by the similar absorption maxima frequencies in the unfolded state and folded state spectra.

According to our previous study on the thermodynamics of GS6,[23] this peptide shows a peculiar thermodynamic behavior: the unfolded state is favored in the whole range of temperatures analyzed, even at low temperatures (280 K). Morover, our data showed that the probability of the folded state rises with the

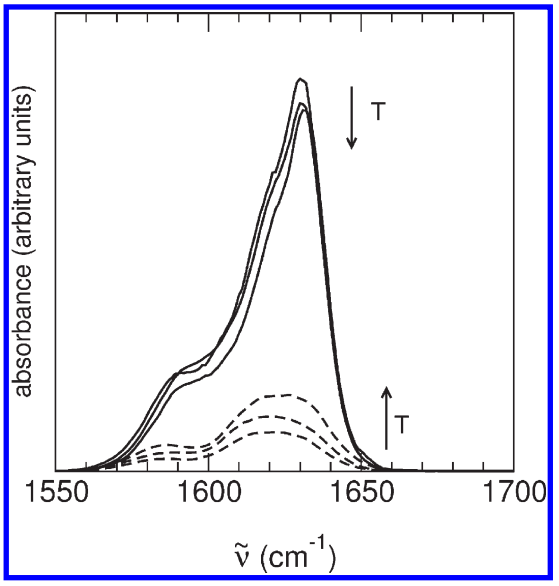

Figure 6. Computed IR spectra in the amide I′ region in D_2O solution of GS6 at 280, 310, and 360 K in the folded state (dashed line) and in the unfolded state (solid line). The height of the curves has been normalized according to the probability of the corresponding state during the MD simulation.

Table 1. GS6 and GS10 Amide I′ Peak Frequencies at 310 K and Percentages of Population in the Unfolded and Folded State As Derived from the Analysis of the MD Trajectory at 310 K

	unfolded state		folded state	
	ν_{peak} (cm^{-1})	population (%)	ν_{peak} (cm^{-1})	population (%)
GS6	1629	84	1620	16
GS10	1647	12	1627	88

temperature up to ≈400 K. The higher population of the unfolded state at every temperature is also evident when comparing the folded and unfolded spectra in Figure 5 with the temperature-dependent spectra (panel A of Figure 3). Indeed, in these last spectra (panel A of Figure 3) it cannot be observed any evidence of a transition from the folded to the unfolded state as the temperature rises: the spectral shape (i.e., the low intensity of the shoulder on the left of the main peak) of the temperature-dependent spectra resembles the spectrum of the unfolded state.

In Figure 6 the spectra of the folded and unfolded state of GS6 are presented with the raising of the temperature. Each spectrum has been weighted with its equilibrium probability obtained by the MD simulation, showing that the folded state probability increases with the raising of the temperature while the opposite trend is observed for the unfolded state. A slight upshift of the main peak can be observed for both states with increasing temperature suggesting that the analogous temperature-dependent upshift of the total spectrum (Figure 3) is an effect of the raising of the temperature and not of a state transition. The different behavior at low temperatures of GS6 and GS10 is also highlighted by Table 1, in which the frequencies of the absorption peaks are reported at 310 K together with the percentages of population in the unfolded and folded state as derived from the analysis of the MD trajectories. It can be observed that, at such temperature, in the case of GS6 the unfolded state is the most populated while the opposite is true for GS10. It can be also observed that the peaks of the folded and unfolded states of GS6 are much more similar in frequency than the ones of GS10. As already commented, this is due to a significant excitonic coupling in the unfolded state.

The comparison between the temperature-dependent spectra of the whole conformational ensemble and the spectra of the strictly folded and unfolded states, as well as the thermodynamic results we previously obtained on the same peptide, suggest that, in the particular case of GS6, the analysis of the temperature-dependent spectra cannot be used to investigate the folding/unfolding kinetics within the usual assumption that the higher the temperature, the higher the probability of the unfolded state. Actually, also the authors of the experimental work observed that the very broad melting transition of GS6 makes it difficult to trust the two-state model fit used to derive the kinetic parameters.[4]

CONCLUSIONS

IR temperature-dependent spectra have been widely used in order to characterize folding/unfolding transitions in peptides and proteins and, more recently, also to characterize folding/unfolding kinetics. In this paper, the experimental temperature-dependent spectra of two small β-hairpin peptides, GS6 and GS10, are reconstructed by means of all-atoms MD simulations and a theoretical−computational approach based on the PMM method. The calculated temperature-dependent spectra well reproduce the experimental ones.

From the analysis of the MD-derived structures, it is possible to define the folded and unfolded states and so to reconstruct also the spectra corresponding to these two conformations. The comparison between the temperature-dependent spectra and the ones corresponding to the folded and unfolded state can be very helpful in order to properly interpret the temperature-dependent spectra, both experimental and calculated. In the case of GS6, for example, it results that the raising of the temperature does not correspond to a transition from the folded to the unfolded state: at every temperature analyzed the spectra match the features of the unfolded state spectrum. This result is also in agreement with a previous study that evidenced a peculiar thermodynamic behavior for GS6: the unfolded state is favored also at low temperatures.[23] In the case of GS10, on the contrary, the spectra at low temperatures correspond to the folded state spectrum while the spectrum at the highest temperature corresponds to the unfolded state one.

AUTHOR INFORMATION

Corresponding Author

*E-mail: andrea.amadei@uniroma2.it.

ACKNOWLEDGMENT

We acknowledge CASPUR (Consorzio Interuniversitario per le Applicazioni di Supercalcolo Per Università e Ricerca) for the use of its computational facilities and its financial support with the project “Theoretical study of electron transfer reactions in complex atomic−molecular systems”.

REFERENCES

(1) Ferguson, N.; Fersht, A. R. *Curr. Opin. Struct. Biol.* **2003**, *13*, 75–81.

(2) Munoz, V.; Thompson, P. A.; Hofrichter, J.; Eaton, W. A. *Nature* **1997**, *390*, 196–199.
(3) Munoz, V.; Henry, E. R.; Hofrichter, J.; Eaton, W. A. *Proc. Natl. Acad. Sci. U.S.A.* **1998**, *95*, 5872–5879.
(4) Maness, S. J.; Franzen, S.; Gibbs, A. C.; Causgrove, T.; Dyer, R. *Biophys. J.* **2003**, *84*, 3874–3882.
(5) Xu, Y.; Oyola, R.; Gai, F. *J. Am. Chem. Soc.* **2003**, *125*, 15388–15394.
(6) Chen, R. P.; Huang, J. J.; Chen, H. L.; Jan, H.; Velusamy, M.; Lee, C. T.; Fann, W.; Larsen, R. W.; Chan, S. I. *Proc. Natl. Acad. Sci. U.S.A.* **2004**, *101*, 7305–7310.
(7) Dyer, R. B.; Maness, S. J.; Peterson, E. S.; Franzen, S.; Fesinmeyer, R. M.; Andersen, N. H. *Biochemistry* **2004**, *43*, 11560–11566.
(8) Du, D.; Zhu, Y.; Huang, C.; Ga, F. *Proc. Natl. Acad. Sci. U.S.A.* **2004**, *101*, 15915–15920.
(9) Dinner, A. R.; Lazaridis, T.; Karplus, M. *Proc. Natl. Acad. Sci. U.S. A.* **1999**, *96*, 9068–9073.
(10) Klimov, D. K.; Thirumalai, D. *Proc. Natl. Acad. Sci. U.S.A.* **2000**, *97*, 2544–2549.
(11) Garcia, A. E.; Sanbonmatsu, K. Y. *Proteins: Struct., Funct., Genet.* **2001**, *42*, 345–354.
(12) Zhou, R.; Berne, B. J.; Germain, R. *Proc. Natl. Acad. Sci. U.S.A.* **2001**, *98*, 14931–14936.
(13) Klimov, D.; Thirumalai, D. *J. Mol. Biol.* **2002**, *315*, 721–737.
(14) Zhou, Y.; Linhananta, A. *Proteins: Struct., Funct., Genet.* **2002**, *47*, 154–162.
(15) Ma, B.; Nussinov, R. *Protein Sci.* **2003**, *12*, 1882–1893.
(16) Bolhuis, P. G. *Proc. Natl. Acad. Sci. U.S.A.* **2003**, *100*, 12129–12134.
(17) Snow, C. D.; Qiu, L.; Du, D.; Gai, F.; Hagen, S. J.; Pande, V. S. *Proc. Natl. Acad. Sci. U.S.A.* **2004**, *101*, 4077–4082.
(18) Roccatano, D.; Amadei, A.; Di Nola, A.; Berendsen, H. J. C. *Protein Sci.* **1999**, *10*, 2130–2143.
(19) Pande, V. S.; Rokhsar, D. S. *Proc. Natl. Acad. Sci. U.S.A.* **1999**, *96*, 9062–9067.
(20) Zagrovic, B.; Sorin, E. J.; Pande, V. *J. Mol. Biol.* **2001**, *313*, 151–169.
(21) Daidone, I.; D'Abramo, M.; Di Nola, A.; Amadei, A. *J. Am. Chem. Soc.* **2005**, *127*, 14825–14832.
(22) Thukral, L.; Smith, J. C.; Daidone, I. *J. Am. Chem. Soc.* **2009**, *131*, 18147–18152.
(23) Zanetti-Polzi, L.; Anselmi, M.; D'Alessandro, M.; Amadei, A.; Di Nola, A. *Biopolymers* **2009**, *91*, 1154–1160.
(24) Plaxco, K. W.; Dobson, C. M. *Curr. Opin. Struct. Biol.* **1996**, *6*, 630–636.
(25) Brockwell, D. J.; Smith, D. A.; Radford, S. E. *Curr. Opin. Struct. Biol.* **2000**, *10*, 16–25.
(26) Schweitzer-Stenner, R. *Vibr. Spectrosc.* **2006**, *42*, 98–117.
(27) Barth, A. *Biochim. Biophys. Acta* **2007**, *1767*, 1073–1101.
(28) Chen, E.; Goldbeck, R. A.; Kliger, D. S. *Annu. Rev. Biophys. Biomol. Struct.* **1997**, *26*, 327–355.
(29) Hahn, S.; Ham, S.; Cho, M. *J. Phys. Chem. B* **2005**, *109*, 11789–11801.
(30) Krimm, S.; Bandekar, J. *Adv. Protein Chem.* **1986**, *38*, 181–364.
(31) Torii, H.; Tasumi, M. *J. Chem. Phys.* **1992**, *96*, 3379–3387.
(32) Lee, S. H.; Krimm, S. *Biopolymers* **1998**, *46*, 283–317.
(33) Ham, S.; Cha, S.; Choi, J. H.; Cho, M. *J. Chem. Phys.* **2003**, *119*, 1451.
(34) Moran, A.; Mukamel, S. *Proc. Natl. Acad. Sci. U.S.A.* **2004**, *101*, 506–510.
(35) Brauner, J. W.; Flach, C. R.; Mendelsohn, R. *J. Am. Chem. Soc.* **2005**, *127*, 100–109.
(36) Yang, S.; Cho, M. *J. Chem. Phys.* **2005**, *123*, 134503.
(37) Bour, P.; Keiderling, T. A. *J. Phys. Chem. B* **2005**, *109*, 23687–23697.
(38) Smith, A. E.; Tokmakoff, A. *J. Chem. Phys.* **2007**, *126*, 045109.
(39) Choi, J. H.; Lee, H.; Lee, K. K.; Hahn, S.; Cho, M. *J. Chem. Phys.* **2007**, *126*, 045102.
(40) Reddy, A.; Wang, L.; Lin, Y.; Ling, Y.; Chopra, M.; Zanni, M.; Skinner, J.; Pablo, J. D. *Biophys. J.* **2010**, *98*, 443–451.
(41) Aschi, M.; Spezia, R.; Di Nola, A.; Amadei, A. *Chem. Phys. Lett.* **2001**, *344*, 374–380.
(42) Spezia, R.; Aschi, M.; Di Nola, A.; Amadei, A. *Chem. Phys. Lett.* **2002**, *365*, 450–456.
(43) Amadei, A.; D'Abramo, M.; Zazza, C.; Aschi, M. *Chem. Phys. Lett.* **2003**, *381*, 187–193.
(44) Amadei, A.; D'Alessandro, M.; D'Abramo, M.; Aschi, M. *J. Chem. Phys.* **2009**, *130*, 084109.
(45) Daidone, I.; Aschi, M.; Zanetti, L.; Nola, A. D.; Amadei, A. *Chem. Phys. Lett.* **2010**, *488*, 213–218.
(46) Amadei, A.; Daidone, I.; Zanetti-Polzi, L.; Aschi, M. *Theor. Chem. Acc.* **2011**, *129*, 31–43.
(47) Zanetti-Polzi, L.; Amadei, A.; Aschi, M.; Daidone, I. *J. Am. Chem. Soc.* **2011**, *133*, 11414–11417.
(48) Cheatum, C.; Tokmakoff, A.; Knoester, J. *J. Chem. Phys.* **2004**, *120*, 8201–15.
(49) Lee, C.; Cho, M. *J Phys. Chem. B* **2004**, *108*, 20397.
(50) Karjalainen, E.; Ravi, H.; Barth, A. *J. Phys. Chem. B* **2011**, *115*, 749–757.
(51) Amadei, A.; Daidone, I.; Di Nola, A.; Aschi, M. *Curr. Opin. Struct. Biol.* **2010**, *20*, 155–161.
(52) Amadei, A.; Marinelli, F.; D'Abramo, M.; D'Alessandro, M.; Anselmi, M.; Di Nola, A.; Aschi, M. *J. Chem. Phys.* **2005**, *122*, 124506.
(53) Gao, J.; Truhlar, D. G. *Annu. Rev. Phys. Chem.* **2002**, *53*, 467–505.
(54) Vreven, T.; Morokuma, K. *Annu. Rep. Comput. Chem.* **2006**, *2*, 35–52.
(55) Senn, H. M.; Thiel, W. *Curr. Opin. Chem. Biol.* **2007**, *11*, 182–187.
(56) Gibbs, A. C.; Kondejewski, L. H.; Gronwald, W.; Nip, A.; Hodges, R.; Sykes, B. D.; Wishart, D. S. *Nat. Struct. Biol.* **1998**, *5*, 284–288.
(57) Gibbs, A. C.; Bjorndahl, T. C.; Hodges, R. S.; Wishart, D. S. *J. Am. Chem. Soc.* **2002**, *124*, 1203–1213.
(58) van Gunsteren, W. F.; Billeter, S.; Eising, A.; Hunenberg, P.; Kruger, P.; Mark, A. E.; Scott, W.; Tironi, I. *Biomolecular Simulations: The GROMOS96 Manual and User Guide*; Hochschulverlag an der ETH Zurich: Zurich, Switzerland, 1996.
(59) Hess, B.; Bekker, H.; Berendsen, H. J. C.; Fraaije, J. G. E. M. *J. Comput. Chem.* **1997**, *18*, 1463–1472.
(60) Berendsen, H. J. C.; van der Spoel, D.; van Drunen, R. *Comput. Phys. Commun.* **1995**, *91*, 43–56.
(61) Berendsen, H. J. C.; Grigera, J. R.; Straatsma, T. P. *J. Phys. Chem.* **1987**, *91*, 6269–6271.
(62) Darden, T.; York, D.; Pedersen, L. *J. Chem. Phys.* **1993**, *98*, 10089–10092.
(63) Brown, D.; Clarke, J. H. R. *Mol. Phys.* **1984**, *51*, 1243–1252.